The proximal promoter region of the human vascular endothelial growth factor gene has a G-quadruplex structure that can be targeted by G-quadruplex–interactive agents

Daekyu Sun,[1] Wei-Jun Liu,[1] Kexiao Guo,[2] Jadrian J. Rusche,[1] Scot Ebbinghaus,[3] Vijay Gokhale,[1] and Laurence H. Hurley[1]

[1]Department of Pharmacology and Toxicology, College of Pharmacy, [2]Department of Biochemistry and Molecular Biophysics, [3]Arizona Cancer Center, and [4]BIO5 Collaborative Research Institute, University of Arizona, Tucson, Arizona

Abstract

Previous studies on the functional analysis of the human vascular endothelial growth factor (*VEGF*) promoter using the full-length *VEGF* promoter reporter revealed that the proximal 36-bp region (−85 to −50 relative to transcription initiation site) is essential for basal or inducible *VEGF* promoter activity in several human cancer cells. This region consists of a polypurine (guanine) tract that contains four runs of at least three contiguous guanines separated by one or more bases, thus conforming to a general motif capable of forming an intramolecular G-quadruplex. Here, we show that the G-rich strand in this region is able to form an intramolecular propeller-type parallel-stranded G-quadruplex structure *in vitro* by using the electrophoretic mobility shift assay, dimethyl sulfate footprinting technique, the DNA polymerase stop assay, circular dichroism spectroscopy, and computer-aided molecular modeling. Two well-known G-quadruplex–interactive agents, TMPyP4 and Se2SAP, stabilize G-quadruplex structures formed by this sequence in the presence of a potassium ion, although Se2SAP is at least 10-fold more effective in binding to the G-quadruplex than TMPyP4. Between these two agents, Se2SAP better suppresses *VEGF* transcription in different cancer cell lines, including HEC1A and MDA-MB-231. Collectively, our results provide evidence that specific G-quadruplex structures can be formed in the *VEGF* promoter region, and that the transcription of this gene can be controlled by ligand-mediated G-quadruplex stabilization. Our results also provide further support for the idea that G-quadruplex structures may play structural roles *in vivo* and therefore might provide insight into novel methodologies for rational drug design. [Mol Cancer Ther 2008;7(4):880–9]

Introduction

The formation of new blood vessels, angiogenesis, is essential for tumor growth and metastasis because it provides oxygen and nutrients to proliferating tumor cells, thus favoring tumor progression (1). The switch to an angiogenic phenotype is mediated by a number of key regulators such as fibroblast growth factors, vascular endothelial growth factors (VEGF), and angiopoietins (2, 3). Among them, VEGF (or VEGF-A) has been considered to be the key mediator of tumor angiogenesis by stimulating the proliferation, migration, survival, and permeability of endothelial cells (4, 5). Recently, a number of agents designed specifically for targeting VEGF and/or its receptors, including antagonistic antibodies, ribozymes, immunotoxins, and synthetic small molecular inhibitors, are being evaluated in various clinical trials in cancer patients (6–15). Whereas a strategy for inhibiting angiogenesis had been proposed more than three decades ago by Folkman (16), basic and translational studies aimed at cultivating a mechanistic understanding of the central role of VEGF in tumor angiogenesis have only recently led to important proof-of-concept clinical trials that convincingly show the benefits of anti-VEGF therapy in patients with advanced cancer (15).

The molecular basis of *VEGF* gene expression has been studied extensively by characterizing the *cis*-acting elements and transcription factors involved in constitutive *VEGF* expression in human cancer cells (17–21). *VEGF* expression is known to be induced by a variety of factors, including hypoxia, pH, activated oncogenes, inactivated tumor suppressor genes, and growth factors (reviewed in ref. 21). These studies revealed that the proximal 36-bp region (−85 to −50 relative to transcription initiation site) is essential for basal or inducible *VEGF* promoter activity in several human cancer cells (21). These *cis*-regulatory elements contain at least three Sp1 binding sites, which consist of guanine/cytosine-rich sequences (Fig. 1A). Although there are binding sites for other factors, such as two Egr-1 elements and one AP-2 element, all Sp1 binding sites were found to be functionally significant in constitutive *VEGF* promoter activity (22). The existence of

Received 11/5/07; revised 1/8/08; accepted 1/21/08.

Grant support: National Cancer Institute/NIH grants CA109069 and CA94166.

The costs of publication of this article were defrayed in part by the payment of page charges. This article must therefore be hereby marked *advertisement* in accordance with 18 U.S.C. Section 1734 solely to indicate this fact.

Requests for reprints: Daekyu Sun, BIO5 Institute, Room 102, 1657 East Helen Street, Tucson, AZ 85721. Phone: 520-626-0323; Fax: 520-626-4824. E-mail: sun@pharmacy.arizona.edu

doi:10.1158/1535-7163.MCT-07-2119

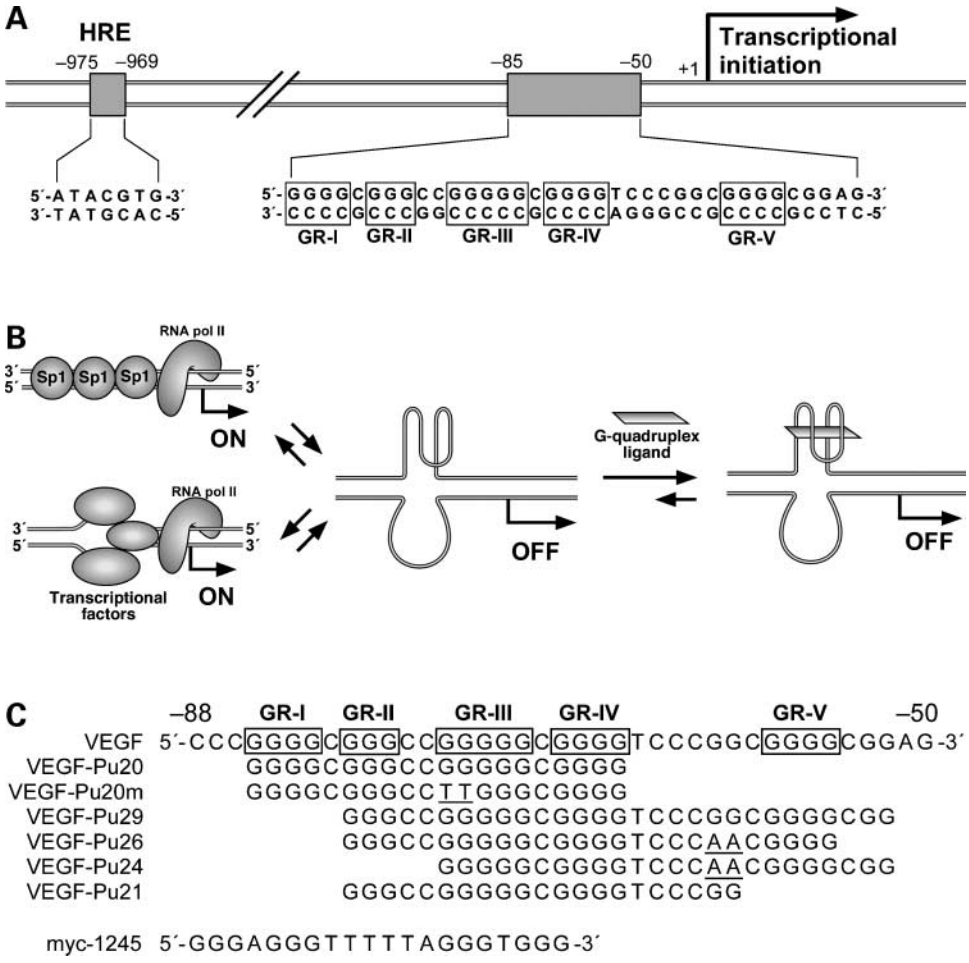

Figure 1. **A,** schematic diagram showing the location of hypoxia response element (*HRE*) and the binding sites for transcription factor Sp1 in the proximal promoter region of the *VEGF* gene. Runs of guanines and cytosines are enclosed in boxes. **B,** models for the repression of *VEGF* gene transcription by G-quadruplex–interactive agents. **C,** oligonucleotides used in this study.

polyguanine/polycytosine tracts in the proximal promoters throughout the human genome has been reported in a number of mammalian genes that are mainly growth related (reviewed in ref. 23). These elements are known to be very dynamic in their conformation, easily adopting non–B-DNA conformations such as melted DNA, hairpin structures, and slipped helices, under physiologic conditions, sometimes even in the absence of conformational or torsional stress (23–32). In particular, G-rich sequences from a number of TATA-less mammalian genes, including *c-MYC, HIF-1α, VEGF, BCL-2, PDGF-A, KRAS, RET*, and *c-KIT*, have been reported to form parallel or antiparallel G-quadruplex structures consisting of two or more G-tetrads in the presence of monovalent cations such as Na^+ and K^+ (24–31). The polypurine tract in the VEGF promoter contains five runs of three or more contiguous guanines separated by one or more bases, conforming to a general motif capable of forming an intramolecular G-quadruplex: G_4 (C) G_3 (CC) G_5 (C) G_4 (TCCCGGC) G_4 (CGG) (ref. 21). In a previous study, we showed that the polypurine/polypyrimidine tracts of the *VEGF* promoter region are very dynamic in structure and can easily adopt a non–B-DNA conformation under physiologic conditions (26). In addition, we predicted that the G-rich strand of this tract could form specific G-quadruplex structures in the presence of K^+ or G-quadruplex–interactive agents. In this report, we showed that the G-rich strand in the proximal promoter region of the *VEGF* gene is capable of forming stable intramolecular G-quadruplex structures *in vitro* and that G-quadruplex–interactive agents such as TMPyP4 and Se2SAP further stabilize these G-quadruplex structures. Moreover, the suppression of *VEGF* transcription was observed in various human cancer cells cultured in the presence of Se2SAP. These results provide support for the idea that G-quadruplex structures may play structural roles *in vivo* and therefore provide insight into novel methodologies for rational drug design by targeting the G-quadruplex structures formed in the *VEGF* promoter (Fig. 1B).

Materials and Methods

Drugs, Enzymes, and Oligonucleotide DNA

TMPyP4, TMPyP2, and Se2SAP were synthesized in our laboratory. Drug molecules were dissolved in DMSO. T4 polymerase kinase and *Taq* DNA polymerase were from

Promega. PAGE-purified oligonucleotides were obtained from Sigma Genosys.

Preparation and End-Labeling of Oligonucleotides

The 5′-end-labeled single-strand oligonucleotides were obtained by incubating the oligonucleotides with T4 polynucleotide kinase and [γ-^{32}P]ATP for 1 h at 37°C. Labeled oligonucleotides were purified with a Bio-Spin 6 chromatography column (Bio-Rad) after inactivation of the kinase by heating at 95°C for 3 min.

Electrophoretic Mobility Shift Assay and Dimethyl Sulfate Footprinting

The ^{32}P-labeled DNA oligomers (100 nmol/L) were denatured by heating at 90°C for 5 min and then cooled slowly to room temperature for 2 to 3 h in 20 mmol/L Tris-HCl buffer with or without 100 mmol/L KCl. Each annealed DNA was treated with dimethyl sulfate (DMS; 1%) for 2 min to methylate DNA. Modification reactions were stopped by adding the same volume of stop buffer containing 50% glycerol and 3 μg of calf thymus DNA, and the modification products were electrophoresed in 1× Tris-borate EDTA buffer on a 16% native polyacryamide gel to separate ssDNA and intramolecular G-quadruplexes from other intermolecular quadruplexes by difference in the electrophoretic mobility. Each species of DNA was isolated from the gel, ethanol precipitated twice, and treated with piperidine (10%). After ethanol precipitation, the cleaved products were resolved on a 16% denaturing polyacrylamide gel.

DNA Polymerase Stop Assay

The template DNAs containing various G-quadruplex–forming regions were annealed with primers (P28) labeled with [γ-^{32}P], and the primer-annealed DNA templates were separated from excess labeled primer or remaining template DNA by electrophoresis through an 8% non-denaturing polyacrylamide gel. The resulting primer-annealed template DNAs were gel purified and used in a primer extension assay by *Taq* DNA polymerase, as previously described (33).

Circular Dichroism Spectroscopy

Circular dichroism (CD) spectra were recorded on a J-810 spectropolarimeter (Jasco) using a quartz cell of 1-mm optical path length and an instrument scanning speed of 100 nm/min, with a response time of 1 s and over a wavelength range of 200 to 330 or 200 to 600 nm for the titration experiments with drugs. All DNA samples were dissolved in Tris-HCl buffer (20 mmol/L, pH 7.6) to a strand concentration of 5 μmol/L. Where appropriate, the samples also contained 100 mmol/L KCl. The CD spectra herein are representations of four averaged scans taken at 25°C and are baseline corrected for signal contributions due to the buffer.

Cell Culture, Drug Treatment, and Reverse Transcription PCR Analysis of the VEGF mRNA Synthesis in Human Cancer Cells

The human breast cancer cell line MDA-MB231, the human endometrial cancer cell line HEC1A, and the human kidney cancer cell lines A498 and 786O were obtained from the American Type Culture Collection. These cell lines were cultured at 37°C in RPMI 1640 (Cellgro) with 10% fetal bovine serum. For the drug treatment of cell lines, exponentially growing cells were plated at $\sim 10^5$/mL in T-75 cm^2 flasks, and drug molecules were added to the media and incubated for the desired times. After drug treatment, the medium in the culture flask was aspirated and the remaining monolayer cells were thoroughly washed once with PBS. The washed cells were trypsinized and harvested for a cell count and, subsequently, for the preparation of total RNA. Total RNA was extracted from cultured cells using RNAwiz (Ambion) according to the manufacturer's protocol. Extracted RNA was pretreated with DNase I (Promega) and reverse transcription was done using oligo(dT)18 primer with RETROscript (Ambion) to generate single-stranded cDNA. Primer sequences for the *VEGF* gene were designed against a common region to all isoforms of the VEGF mRNA: forward primer, 5′-TGCATTGGAGCCTTGCCTTG-3′ (nucleotides 1,054–1,073 from NM 003376.4); reverse primer, 5′-CGGCTCACCGCCTCGGCTTG-3′ (nucleotides 1,664–1,683 from NM 003376.4). In parallel, the amplification of β-actin cDNA was done as an internal standard according to the manufacturer's protocol (Ambion). All of the reactions involved an initial denaturation at 95°C for 3 min, followed by 40 cycles for VEGF or 30 cycles for β-actin at 94°C for 30 s, 55°C for 30 s, and 72°C for 40 s on a GeneAmp PCR system 9600 (Perkin-Elmer).

Results

Formation of Intramolecular G-Quadruplex Structures by the G-Rich Strand of the VEGF Proximal Promoter Region

The G-rich strand (−85 to −50) of the VEGF promoter is characterized by the presence of five runs of at least three adjacent guanines, which we designated GR-I through GR-V (Fig. 1A). To determine which guanine repeats were required for folding into intramolecular G-quadruplex structures, we prepared a series of DNA oligonucleotides spanning various portions of the G-rich sequence (Fig. 1C), as described in the Materials and Methods. It is well known that the guanine bases involved in the formation of G-quadruplex structures are inaccessible to methylation because the N7 positions of those guanines are involved in Hoogsteen bonding to form the G-tetrad (24). The methylated oligos were then subjected to a native PAGE to separate intramolecular G-quadruplexes from other intermolecular quadruplexes by differences in electrophoretic mobility. As shown in Fig. 2A, a native gel electrophoresis of the 5′-end-labeled VEGF-Pu20 incubated in the presence of 100 mmol/L KCl resulted in the formation of one major band (band 5 in Fig. 2A), whereas two major bands were formed in the absence of KCl (bands 3 and 4 in Fig. 2A). Each DNA was excised from the gel and treated with piperidine, and the cleavage products were resolved on a sequencing gel. The pattern of N7 guanine methylation produced by band 5 is consistent with the an intramolecular quadruplex containing three stacked G-tetrads

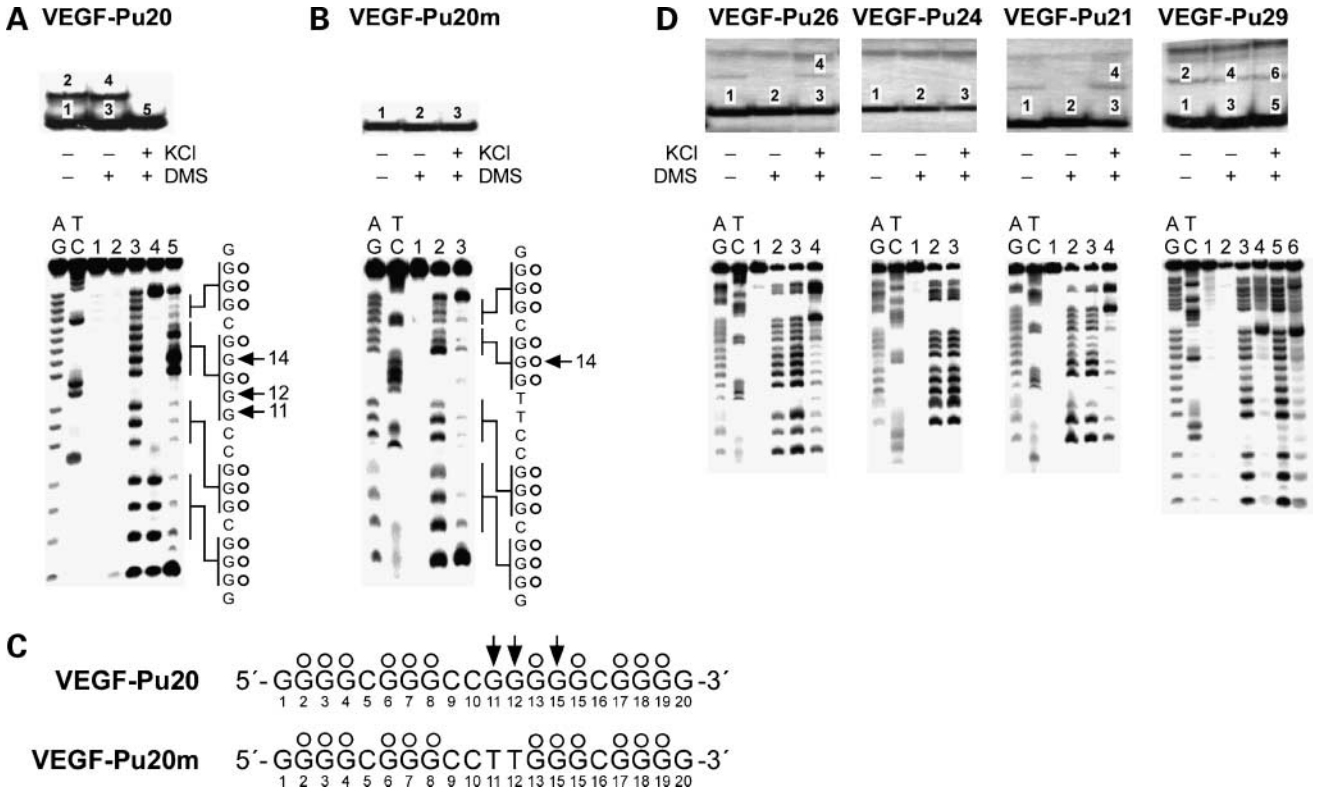

Figure 2. Determination of the intramolecular G-quadruplex structures formed by the G-rich sequence of the VEGF promoter region in the presence of 100 mmol/L KCl. **A,** *top,* EMSA of VEGF-Pu20 preincubated under the conditions specified in the figure using 16% native polyacrylamide gel. *Bottom,* DMS footprinting of each band (*1 – 5*) from EMSA. *AG* and *TC,* sequencing lanes; *lanes 1* to *5,* bands from EMSA. **B,** *top,* EMSA of VEGF-Pu20m preincubated under the conditions specified in the figure using 16% native polyacrylamide gel. *Bottom,* DMS footprinting of each band (*1 – 3*) from EMSA. *AG* and *TC,* sequencing lanes; *lanes 1* to *3,* bands from EMSA. The vertical bars to the left of lane 5 (**A**) and lane 3 (**B**) correspond to DMS-protected guanine repeats, and the sequences to the right show the protected guanines (○). **C,** summary of DMS footprinting of VEGF-Pu20 and VEGF-Pu20m in the presence of 100 mmol/L KCl. The protected guanines from DMS are indicated by open circles, and guanine residues hypermethylated by DMS are indicated by arrowheads. **D,** determination of the structures of G-quadruplexes formed from VEGF-Pu26, Pu24, Pu21, and Pu29 in the presence of 100 mmol/L KCl. *Top,* EMSA of VEGF-Pu26, Pu24, Pu21, and Pu29 (*left* to *right*) preincubated under the conditions specified in the figure using 16% native polyacrylamide gel. *Bottom,* DMS footprinting of each band from EMSA. *AG* and *TC,* sequencing lanes; each lane corresponds to the bands from corresponding EMSA.

(Fig. 2A, *lane 5*). However, the DMS cleavage pattern of band 3 corresponds to that of the single-stranded form (Fig. 2A, *lane 3*), whereas band 4 (Fig. 2A, *lane 4*) is believed to be an intermolecular G-quadruplex due to its much slower electrophoretic mobility compared with the intramolecular form of G-quadruplex structure (band 5). The formation of intermolecular G-quadruplex structures under salt-deficient conditions in VEGF-Pu20 is intriguing. However, we speculate that intermolecular G-quadruplex formation in VEGF-Pu20 under salt-deficient conditions during gel electrophoresis could still be facilitated by the small amounts of sodium ions (2–3 mmol/L) present in Tris-borate EDTA buffer. DMS cleavage of band 5 showed that three stacked G-tetrads formed by four G-stretches were protected from the methylation by DMS (except G14), whereas guanine residues G11 and G12, within the central loop (in sequence to right of lane 5 in Fig. 2A) showed hypersensitivity to DMS. To probe the effect of mutation of these guanines which show hypersensitivity to DMS, a mutant oligomer (VEGF-Pu20m in Fig. 2B) was investigated. The DMS cleavage at the G14 residue of VEGF-Pu20 disappeared when G11 and G12, within the central loop were replaced with thymine residues in VEGF-Pu20m (Fig. 2B, *lane 3*), indicating a possible interaction of this guanine residue with bases within the central 4-base loop. Overall, the results from this study suggest the strong tendency of VEGF-Pu20 to form an intramolecular G-quadruplex structure in the presence of KCl while forming either single-stranded structures or intermolecular G-quadruplex structures in the absence of KCl. The results of DMS footprinting for VEGF-Pu20 and VEGF-Pu20m in the presence of 100 mmol/L KCl are summarized in Fig. 2C.

In contrast to VEGF-Pu20, the major band of the other oligonucleotides (VEGF-Pu26, VEGF-Pu24, VEGF-Pu21, and VEGF-Pu29) incubated in the presence of 100 mmol/L KCl failed to show the N7 guanine protection from methylation, indicating that these oligonucleotides do not form intramolecular G-quadruplexes (see lane 5 for VEGF-Pu29 and lane 3 for VEGF-Pu26, VEGF-Pu24, and VEGF-Pu21 in

Fig. 2D). Only the minor band with lower electrophoretic mobility (band 4 or 6 in Fig. 2D) representing intermolecular G-quadruplexes exhibited the protection of guanine residues from DMS (see lanes 4 and 6 for VEGF-Pu29 and lane 4 for VEGF-Pu26 and VEGF-Pu21 in Fig. 2D), suggesting that these structures form only intermolecular G-quadruplexes. Collectively, these results indicate that the intramolecular G-quadruplex formed within the G-rich sequence of the VEGF promoter requires four G blocks (GR-I to GR-IV), consisting of 12 guanines, whereas other G blocks such as GR-V may be required for the formation of an intermolecular G-quadruplex, which is less likely to be biologically relevant.

Sequence VEGF-Pu20 Forms an Intramolecular Propeller-Type Parallel-Stranded G-Quadruplex

Like the G-quadruplex formed from four consecutive human telomeric DNA repeats (34), the sequence myc-1245, a mutant type of the Pu27-mer from the NHE III_1 of the c-myc (see Fig. 3A), was shown by NMR to form a stable intramolecular propeller-type parallel-stranded G-quadruplex in K^+-containing solution (35). To compare the structure formed from VEGF-Pu20 with that of myc-1245, we first determined the number of stacked G-tetrads and the guanines involved in the G-quadruplex structure formed by myc-1245 by using electrophoretic mobility shift assay (EMSA) and the DMS footprinting method. As shown in Fig. 3B and C, the DMS footprinting experiment revealed that this structure involves a core of three stacked G-tetrads formed by four G-stretches with three loops bridging the three the G-tetrad layers, conforming to the folding pattern determined by the NMR (35). The central loop contains six residues, each whereas the two other loops contain only one residue each. Next, the CD spectra of VEGF-Pu20 and myc-1245 were compared to determine the direction of the backbone (e.g., antiparallel or parallel orientation) in the G-quadruplex structure formed by VEGF-Pu20 because CD spectroscopy has been widely used to infer the presence of G-quadruplexes and is particularly useful for differentiating parallel and antiparallel G-quadruplexes (36, 37). All guanosines in the structure of a parallel quadruplex have an *anti* conformation of the glycosyl bonds, resulting in a positive band at ~265 nm and a small negative band at ~245 nm in a CD spectrum (36, 37). In contrast, the guanosines in an antiparallel quadruplex have alternating *syn*- and *anti*-glycosyl conformations along each strand, exhibiting a positive band at ~295 nm that is associated with an antiparallel strand arrangement. As shown in Fig. 3D, the CD spectra of both sequences showed a positive band at ~265 nm and a small negative band at ~245 nm in K^+-containing solution, which is consistent with a parallel structure (36, 37).

Models for G-Quadruplex Structures Formed in the G-Rich Strand of the VEGF Promoter

On the basis of information obtained from this study using biochemical and biophysical methods, including EMSA, DMS footprinting, and CD spectroscopy, we have

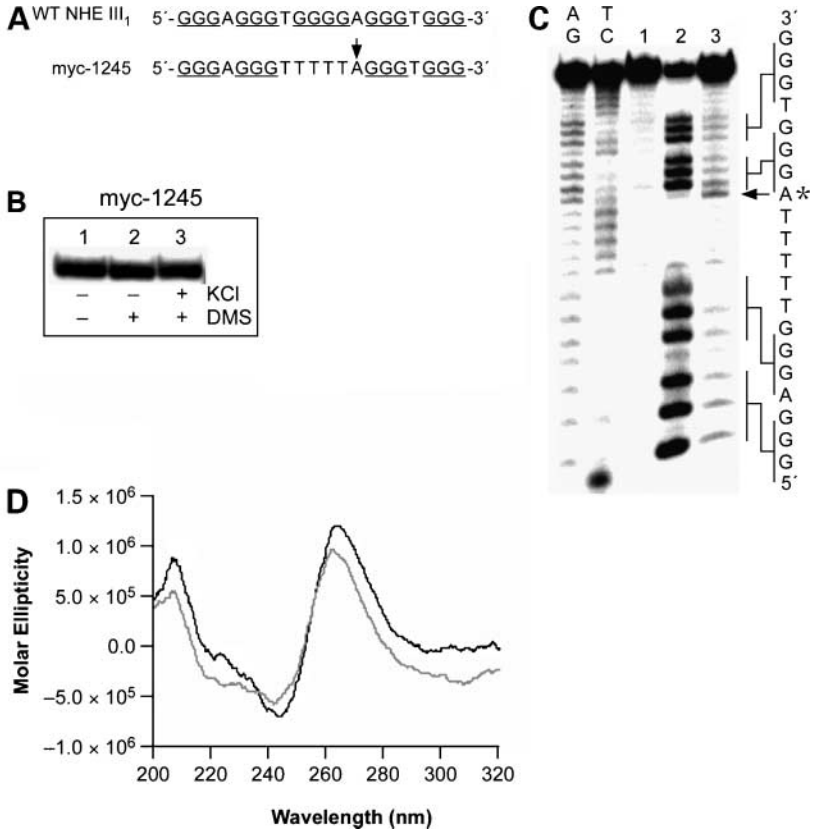

Figure 3. EMSA, DMS footprinting of VEGF-Pu20, and CD spectrum of the sequence myc-1245. **A,** sequence of the wild-type (WT) and mutant (myc-1245) NHE III_1 in the C-MYC promoter. **B,** EMSA of the sequence myc-1245 preincubated under the conditions specified in the figure using a 16% native polyacrylamide gel. **C,** DMS footprinting of each band from EMSA. **D,** CD spectra of the myc-1245 (*solid line*) in comparison with that of VEGF-Pu20 (*dashed line*). The CD data were obtained with a 5 μmol/L strand concentration in the presence of 100 mmol/L KCl at 25°C.

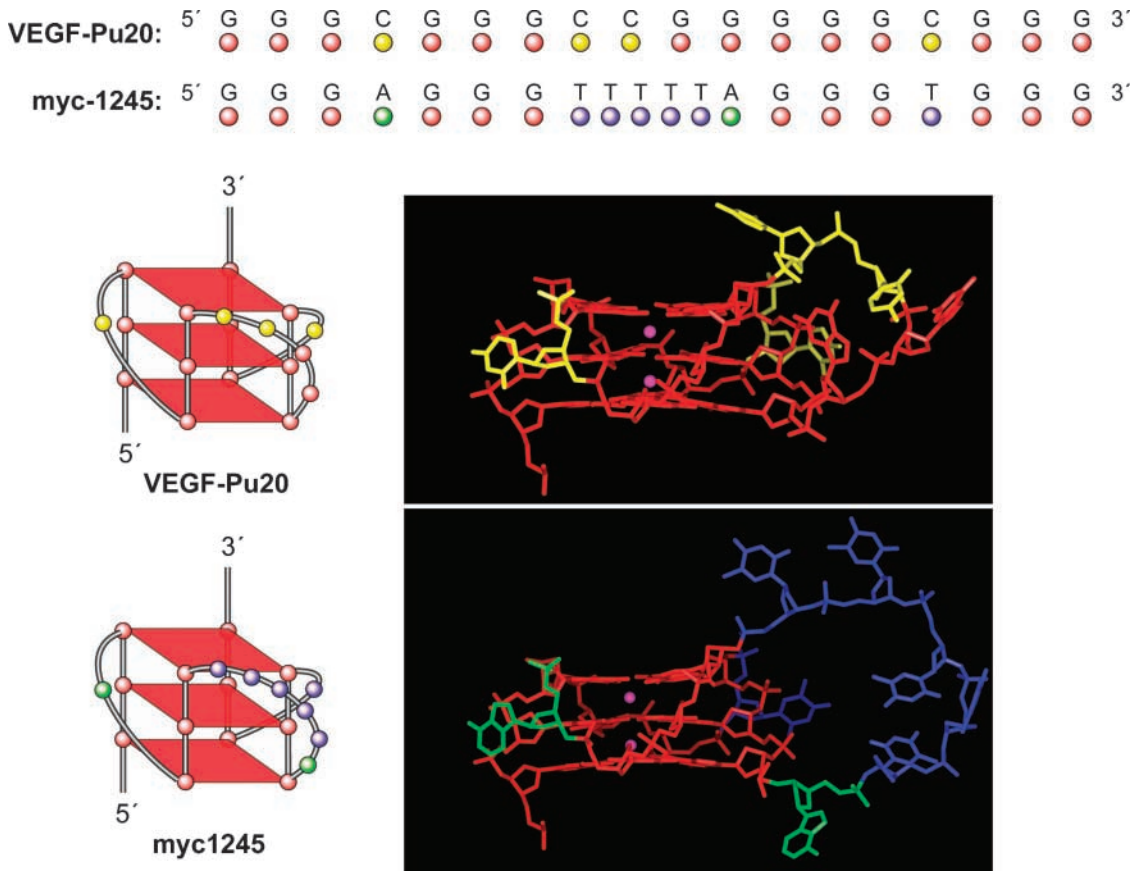

Figure 4. Molecular modeling structures for G-quadruplexes formed by VEGF-Pu20 in comparison with the known folding pattern of myc-1245. *Top*, alignment of both sequences. *Middle,* schematic illustration (*left*) and molecular modeling structure (*right*) of the VEGF parallel quadruplex. *Bottom,* schematic illustration (*left*) and molecular modeling structure (*right*) of the myc-1245 parallel quadruplex. The structure of the human c-myc parallel quadruplex was used as a starting structure (35). Necessary replacements and deletions were done. Loop geometries were obtained as in the case of the human telomeric DNA parallel quadruplex (PDB code 1KF1; ref. 34). Modeling was done using the Biopolymer module within the Insight II modeling software and charges, and potential types were assigned using the Amber force field within Insight II (Accelrys). Structures were minimized using 2,500 steps of Discover 3 (Accelrys) minimization as previously described (42).

determined the number of stacked G-tetrads, the guanines involved in the G-quadruplex, and the probable direction of the backbone (e.g., antiparallel or parallel orientation) in the major G-quadruplex structures formed by the G-rich sequence in the promoter region of the *VEGF* gene. In the sequence myc-1245 examined by the Patel group (35), there are two 1-base loops analogous to those found in the VEGF sequences flanking a 6-thymine-base loop analogous to the 4-base loop in the VEGF sequence (Fig. 4). Therefore, the principal differences between the VEGF sequence and myc-1245 are the size (4 versus 6) and identity of the bases (purines versus pyrimidines) in the central loop. This analogous sequence provides some insight into the probable folding pattern of the VEGF G-quadruplex structures. The myc-1245 structure involves a core of three stacked G-tetrads formed by four parallel G-stretches with all *anti* conformations in the nucleosides and three double-chain-reversal loops bridging three G-tetrad layers (Fig. 4). Although VEGF-Pu20 and myc-1245 contain different sets of G-stretches, their overall folding topologies look strikingly similar, with a parallel-stranded G-tetrad core and three double-chain-reversal loops, two of which are one-residue loops. These G-quadruplexes were found to be stable during molecular minimization and dynamics calculations (Fig. 4). All of the nucleotides of the tetrads exist in an *anti* conformation. Single-base loops connecting parallel guanine strands, as well as all guanine bases of the strands connected by single-base loops in the tetrad arrangement, were found to be stable. The main difference between the two structures lies in the size and sequence of the central loop, which is a four-residue loop in VEGF-Pu20 and a six-residue loop in myc-1245 (see Fig. 4).

G-Quadruplex–Interactive Agents Stabilize an Intramolecular G-Quadruplex Structure Formed by the G-Rich Strand of the VEGF Proximal Promoter Regions

To test whether G-quadruplex–interactive agents stabilize an intramolecular G-quadruplex structure formed

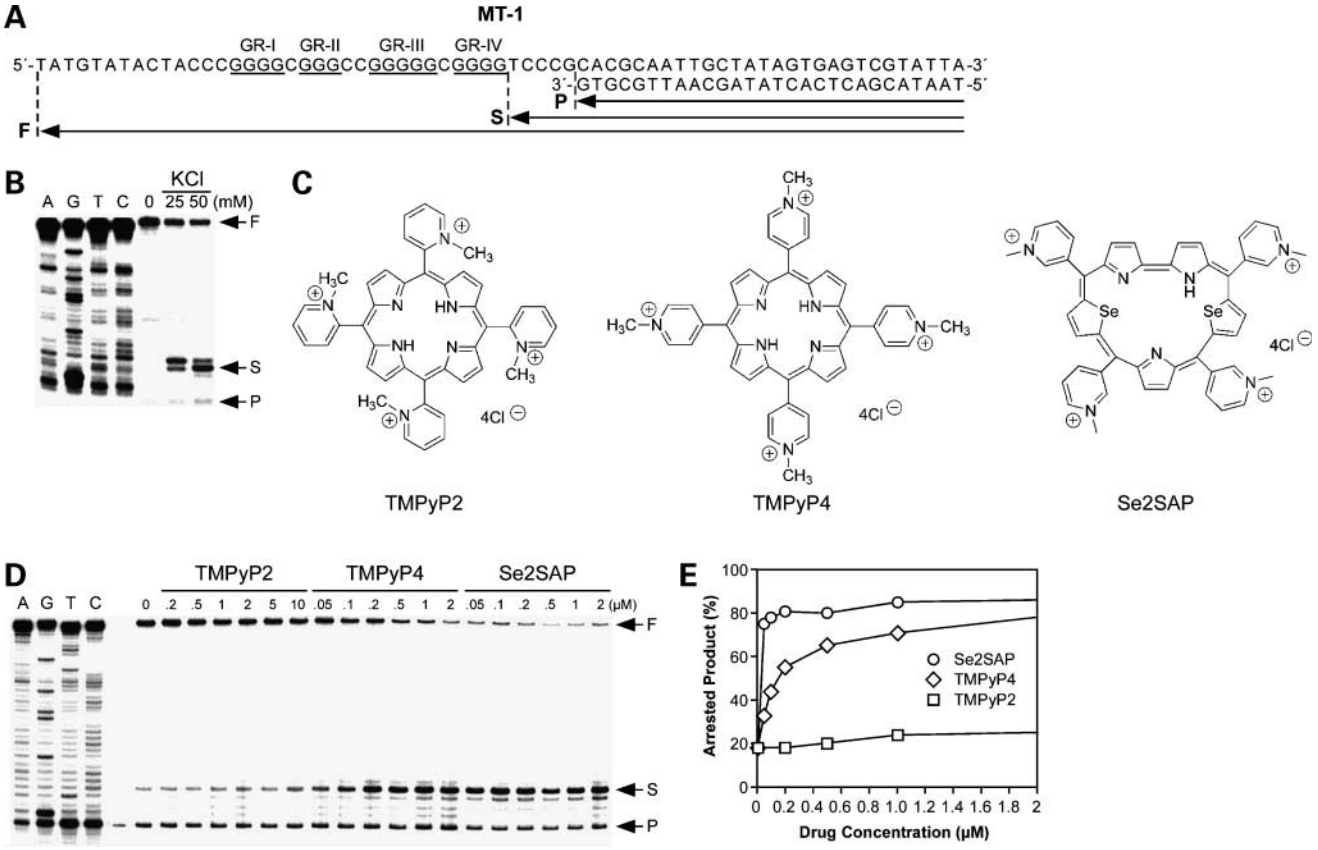

Figure 5. *Taq* DNA polymerase stop assay showing the stabilization of G-quadruplex structures by KCl and TMPyP2, TMPyP4, and Se2SAP. **A,** sequence of the ssDNA template annealed with the primer used in the DNA polymerase stop assay. **B,** KCl-dependent pausing of DNA polymerase DNA synthesis at the 3′ side of the fourth guanine run in the DNA template containing the VEGF-Pu20 sequence. **C,** structures of TMPyP2, TMPyP4, and Se2SAP. **D,** *left,* stabilization of G-quadruplex structure formed by VEGF-Pu20 with the addition of increasing concentrations of TMPyP2, TMPyP4, and Se2SAP. *Arrows,* positions of the full-length product (*F*) of DNA synthesis, the G-quadruplex stop sites (*S*), and the free primer (*P*). *Lanes A, G, T,* and *C,* dideoxysequencing reactions with the same template as the size marker for the precise arrest sites. *Right,* percentage of the major arrest products of each sample to the total product was plotted against drug concentration.

by the G-rich strand of the VEGF proximal promoter region, a DNA polymerase stop assay was used with a DNA template (MT-1 in Fig. 5A) containing VEGF-Pu20 annealed with ^{32}P-labeled primers. Figure 5B shows a potassium-dependent pause of DNA polymerase extension through this DNA template at 37°C. In the absence of KCl, the DNA polymerase bypasses the G-repeat region; however, in the presence of KCl, pausing is observed immediately 3′ to the fourth guanine run (GR-IV; see Fig. 5A), presumably by stabilizing the intramolecular G-quadruplex structure, confirming that this region is indeed capable of forming intramolecular G-quadruplex structures. We next examined two well-known G-quadruplex-interactive agents (TMPyP4 and Se2SAP; Fig. 5C) for their ability to interact with the G-quadruplex using the polymerase stop assay. TMPyP4 is a cationic porphyrin that has been shown to interact specifically with G-quadruplexes, and Se2SAP is a core-modified expanded porphyrin analogue with significantly reduced photoreactivity compared with TMPyP4 and TMPyP2. These G-quadruplex–interactive agents used in this experiment have been described in our previous studies (30, 33, 34, 37–39). These agents are capable of interacting with the G-quadruplex in the *VEGF* promoter as shown by a concentration-dependent increase in the amount of arrest compared with the amount of arrest seen with potassium alone, suggesting that these agents stabilize the G-quadruplex formed by this sequence (Fig. 5D, *left*). Interestingly, Se2SAP turned out be at least 10-fold more effective in binding to the *VEGF* G-quadruplex than TMPyP4. In contrast, TMPyP2 (structure shown in Fig. 5C), a structural isomer of TMPyP4 that is known to have low affinity for G-quadruplexes due to its inability to enter or stack into G-tetrad structures (40), had little effect on the formation of the arrest products (Fig. 5D, *right*).

The G-Quadruplex–Interactive Agent Se2SAP Causes a Decrease in the Expression of VEGF in Human Tumor Cells

Having shown that the G-rich strand of Sp1 binding sites within the *VEGF* promoter region is capable of forming

intramolecular G-quadruplex structures *in vitro* and that G-quadruplex–interactive agents further stabilize these G-quadruplex structures, we next determined whether the expression of the *VEGF* gene is affected by G-quadruplex–interactive agents in various human cancer cell lines, including kidney (A498 and 786-O), endometrial (HEC1A), and breast (MDA-MB231) cancers. As shown in Fig. 6A and B, Se2SAP decreased *VEGF* gene expression by 50% and 80% in MDA-MB231 and HEC1A cells, respectively, at 48 h posttreatment. This compound also decreased *VEGF* gene expression in two kidney cell lines, A498 and 786-O, by 50% to 60% within 24 h after treatment (Fig. 6C and D). In contrast, TMPyP2 has little effect on the expression of the *VEGF* gene at the range of concentrations used, although this resulted in similar growth inhibition of these cell lines by TMPyP4 and Se2SAP (data not shown), suggesting that the transcriptional repression of *VEGF* gene by G-quadruplex–interactive agents is not simply a result of decreased proliferation of HEC1A cells. TMPyP4, which is less effective in binding to the VEGF G-quadruplex than Se2SAP, has only a marginal effect on the inhibition of *VEGF* expression in HEC1A cell lines, although it is capable of interacting with VEGF intramolecular G-quadruplex structures. Therefore, a substantial difference between the different G-quadruplex–interactive agents in binding affinity to G-quadruplexes could be attributed to their varying degrees of potency in down-regulating *VEGF* expression.

Discussion

In an expanding tumor mass, *VEGF* expression is physiologically induced in many tumor types by hypoxia and hypoglycemia, particularly in regions surrounding necrosis (4, 5). In addition, tumor cells may produce VEGF in the absence of physiologic stimuli due to the loss of tumor suppressor genes, such as *VHL* and *p53*, the activation of certain growth factor signaling cascades, such as epidermal growth factor receptor, and the stimulation of tumor cells by cytokines, growth factors, gonadotropins, and several other extracellular molecules from normal or malignant cells, which act in an endocrine, paracrine, or autocrine fashion (17–26). Thus, VEGF and its receptors are regarded as potential targets for therapeutic intervention (6–8).

In this study, we explored a potentially new strategy to inhibit the production of VEGF in tumor cells by targeting the G-quadruplex structures formed by the G-rich sequences in the promoter region of the *VEGF* gene. Direct evidence for the existence of G-quadruplexes *in vivo* is beginning to emerge, and the ability of some of the G-rich sequences to form very stable G-quadruplex structures *in vitro* suggests that G-quadruplex DNA may play an important role in several biological events (29–34). For instance, an earlier study provided compelling evidence that a specific G-quadruplex structure formed in the c-myc promoter functions as a transcriptional repressor element, establishing the principle that c-myc transcription can be controlled by ligand-mediated G-quadruplex stabilization

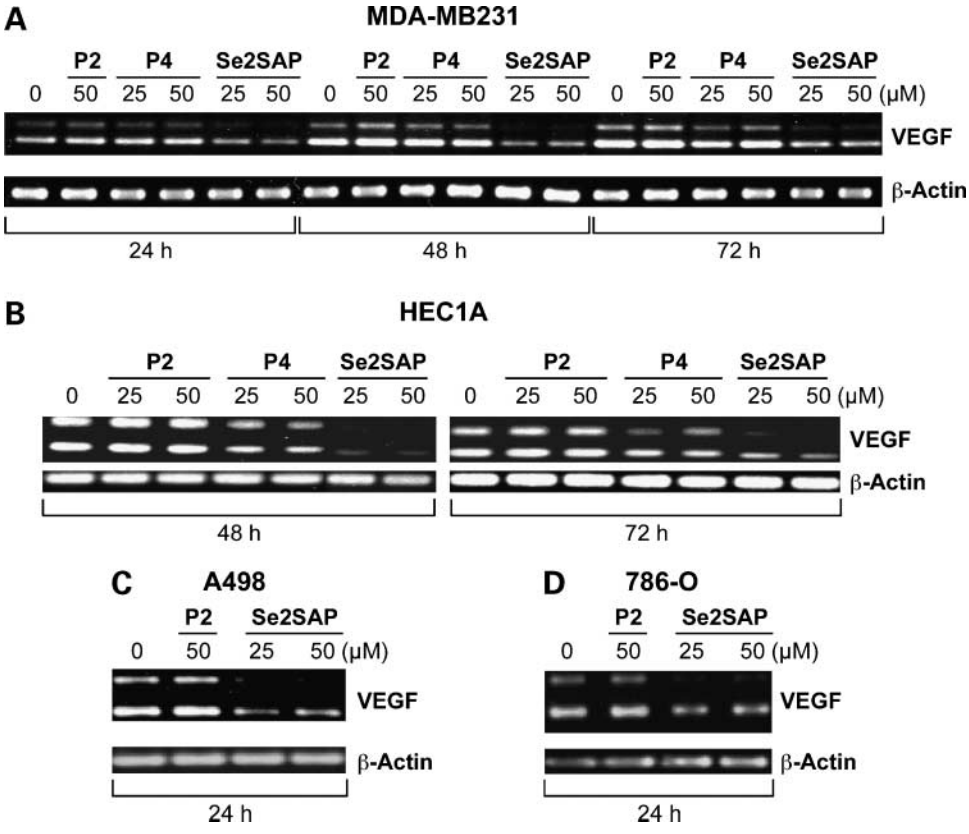

Figure 6. Effect of G-quadruplex–interactive agents on *VEGF* mRNA synthesis in the MDA-MB231 cell line (**A**), HEC1A (**B**), A498 (**C**), and 786-O (**D**). Human cancer cells were treated with TMPyP2 (P2), TMPyP4 (P4), and Se2SAP at various concentrations for indicated times, and *VEGF* mRNA and β-actin mRNA were measured by reverse transcription PCR. Less than 30% reduction in the number of cells occurred over 3 d after treatment with 50 μmol/L of TMPyP4, TMPyP2, and Se2SAP (data not shown). Two products were obtained after reverse transcription PCR, which correspond to c-DNAs of $VEGF_{121}$ and $VEGF_{165}$.

(24). This principle has now been independently confirmed by a second group using structurally distinct molecules (41). More recently, the folding pattern (35) and solution structure (42) of the parallel G-quadruplex in the c-myc promoter resulting from the four 3′ runs of guanines in the NHE III_1 have been determined. Significantly, this G-quadruplex has a melting point of >85°C and is a mixture of four loop isomers.

The promoter element encompassing the three Sp1 binding sites contains five runs of three or more contiguous guanines (Fig. 1A) and has a potential to form two alternative intramolecular G-quadruplex structures. Of these alternative structures, that involving the four 5′ runs of guanines seems to be the most stable. In the absence of the four terminal 5′ guanines, neither of the G-quadruplex structures is able exist in a stable form. Within the four 5′ runs of guanines, the second has only three guanines, limiting the G-quadruplex to three tetrads. DMS footprinting confirms the formation of a G-quadruplex containing three tetrads, although there is one anomaly in the second run of three guanines, which we shall discuss later. The results from CD spectroscopy suggests that the G-quadruplex is a parallel G-quadruplex and the two single nucleotides (C) that separate the DMS-protected runs of three guanines suggest the presence of two double-chain reversal loops similar to those found in the myc-1245 structure. In this mutant sequence derived from the NHE III_1 in the *c-myc* promoter, the central run of guanines is substituted with four thymines (Fig. 3A). However, in the case of VEGF, the second loop contains four nucleotides (CCGG), of which the two guanines show hypersensitivity to DMS. Overall, the DMS (Fig. 2A) and CD (Fig. 3D) characteristics of this sequence closely align to those associated with the folding pattern of a c-myc myc-1245 in which there are three double-chain reversal loops containing 1, 6, and 1 nucleotides. In comparison, the VEGF core sequence has 1-, 4-, and 1-nucleotide loops. An unexplained property of the DMS cleavage pattern is the cleavage of a guanine in the central tetrad that disappears on substitution of the two guanines in the 4-base loop with thymine bases (compare Fig. 2A and B). This is suggestive of a central modified tetrad structure of as yet undetermined structure, which could be determined by NMR in a separate study.

The second important goal of this study was to provide proof of principle that G-quadruplex–interactive agents could be potentially used as a new class of antiangiogenic agents by inhibiting the transcriptional activity of the *VEGF* gene. Therefore, we used the G-quadruplex–interactive agents TMPyP4 and Se2SAP in our initial studies because previous studies clearly showed that these compounds showed varying degrees of selectivity for G-quadruplexes over duplex or other forms of secondary structures (30, 33, 34, 37–39). As described in the Results section, Se2SAP, compared with TMPyP4, was proven highly effective in binding to the VEGF G-quadruplex. Significantly, Se2SAP was also very effective in inhibiting *VEGF* transcription in various human cancer cell lines, including HEC1A, MDA-MB231, A498, and 786-O, although some variation in the degree of inhibition of *VEGF* gene expression with Se2SAP was observed between the cell lines. To avoid general cytotoxic effects, TMPyP2 was dosed at the same range of concentrations that resulted in similar growth inhibition of these cell lines by TMPyP4 and Se2SAP. At these concentrations, TMPyP2 had little effect on the expression of *VEGF*.

The spatial distribution of expressed VEGF isoforms is known to vary both within and between tumor types, although $VEGF_{121}$ and $VEGF_{165}$ seem to predominate in human cancer (43). We observed that the expression of $VEGF_{121}$ was the most predominant in all cell lines, whereas the expression of $VEGF_{165}$ varied between cell lines (low in MDA-MB231, A498, and 786-O cell lines and higher in HEC1A cell line). Because Se2SAP suppresses the expression of both VEGF mRNA isoforms in these cell lines, our data suggest that G-quadruplex–interactive agents would have little influence on the splicing process of VEGF mRNA isoforms. Whereas it is attractive to suggest a mechanism in which the G-quadruplex–interactive compounds such as Se2SAP down-regulate VEGF by direct interaction with the G-quadruplex in the promoter region, thereby inhibiting transcriptional activation, we cannot at this time rule out alternative mechanisms.

In summary, to develop a new potential strategy to inhibit the production of VEGF in tumor cells, we characterized specific G-quadruplex structures formed in the *VEGF* promoter region and determined whether the transcription of this gene can be controlled with G-quadruplex–interactive agents targeting the G-quadruplex structure formed by the G-rich sequences in the promoter region of the *VEGF* gene. We showed that the G-rich strand in this region are able to form intramolecular G-quadruplex structures *in vitro*, which are further stabilized by G-quadruplex–interactive agents. These agents are able to suppress *VEGF* transcription in human tumor cells, raising the possibility that a new antiangiogenic therapy can be developed by targeting specific G-quadruplex structures formed in the promoter region of the *VEGF* gene and inhibiting the transcription of this gene with G-quadruplex–interactive agents. Thus, the identification of novel antiangiogenic compounds based on G-quadruplex–interactive agents could have important applications in the treatment of human cancers. Furthermore, the combination of certain G-quadruplex–interactive agents with a number of recently developed agents for targeting VEGF and/or its receptors (6–15) with different mechanisms of action is likely to produce an enhanced antiangiogenic effect in human cancer.

Acknowledgments

We thank Dr. Sridevi Bashyam (University of Arizona) for synthesizing Se2SAP for this study, and David Bishop for preparing, proofreading, and editing the final version of the manuscript and figures.

References

1. Folkman J. Role of angiogenesis in tumor growth and metastasis. Semin Oncol 2002;29:15 – 8.

2. Sullivan DC, Bicknell R. New molecular pathways in angiogenesis. Br J Cancer 2003;89:228 – 31.

3. Giordano FJ, Johnson RS. Angiogenesis: the role of the microenvironment in flipping the switch. Curr Opin Genet Dev 2001;11:35 – 40.

4. Goodsell DS. The molecular perspective: VEGF and angiogenesis. Stem Cells 2003;21:118 – 9.

5. Jain RK. Tumor angiogenesis and accessibility: role of vascular endothelial growth factor. Semin Oncol 2002;29:3 – 9.

6. Sato Y. Molecular diagnosis of tumor angiogenesis and anti-angiogenic cancer therapy. Int J Clin Oncol 2003;8:200 – 6.

7. Martiny-Baron G, Marme D. VEGF-mediated tumour angiogenesis: a new target for cancer therapy. Curr Opin Biotechnol 1995;6:675 – 80.

8. Bikfalvi A, Bicknell R. Recent advances in angiogenesis, anti-angiogenesis and vascular targeting. Trends Pharmacol Sci 2002;23:576 – 82.

9. Sepp-Lorenzino L, Thomas KA. Antiangiogenic agents targeting vascular endothelial growth factor and its receptors in clinical development. Expert Opin Investig Drugs 2002;11:1447 – 65.

10. Niederman TM, Ghogawala Z, Carter BS, et al. Antitumor activity of cytotoxic T lymphocytes engineered to target vascular endothelial growth factor receptors. Proc Natl Acad Sci U S A 2002;99:7009 – 14.

11. Jin N, Chen W, Blazar BR, et al. Gene therapy of murine solid tumors with T cells transduced with a retroviral vascular endothelial growth factor-immunotoxin target gene. Hum Gene Ther 2002;13:497 – 508.

12. Stefanik DF, Fellows WK, Rizkalla LR, et al. Monoclonal antibodies to vascular endothelial growth factor (VEGF) and the VEGF receptor, FLT-1, inhibit the growth of C6 glioma in a mouse xenograft. J Neurooncol 2001; 55:91 – 100.

13. Hess C, Vuong V, Hegyi I, et al. Effect of VEGF receptor inhibitor PTK787/ZK222584 [correction of ZK222548] combined with ionizing radiation on endothelial cells and tumour growth. Br J Cancer 2001;85: 2010 – 16.

14. Holash J, Davis S, Papadopoulos N, et al. VEGF-Trap: a VEGF blocker with potent antitumor effects. Proc Natl Acad Sci USA 2002;99: 11393 – 8.

15. Yang JC, Haworth L, Sherry RM, et al. A randomized trial of bevacizumab, an anti-vascular endothelial growth factor antibody, for metastatic renal cancer. N Engl J Med 2003;349:427 – 34.

16. Folkman J. Tumor angiogenesis: therapeutic implications. N Engl J Med 1971;285:1182 – 6.

17. Schafer G, Cramer T, Suske G, et al. Oxidative stress regulates vascular endothelial growth factor-A gene transcription through Sp1- and Sp3-dependent activation of two proximal GC-rich promoter elements. J Biol Chem 2003;278:8190 – 8.

18. Maeno T, Tanaka T, Sando Y, et al. Stimulation of vascular endothelial growth factor gene transcription by all trans retinoic acid through Sp1 and Sp3 sites in human bronchioloalveolar carcinoma cells. Am J Respir Cell Mol Biol 2002;26:246 – 53.

19. Pal S, Datta K, Mukhopadhyay D. Central role of p53 on regulation of vascular permeability factor/vascular endothelial growth factor (VPF/VEGF) expression in mammary carcinoma. Cancer Res 2001; 61:6952 – 57.

20. Pal S, Datta K, Khosravi-Far R, et al. Role of protein kinase Cζ in Ras-mediated transcriptional activation of vascular permeability factor/ vascular endothelial growth factor expression. J Biol Chem 2001;276: 2395 – 403.

21. Loureiro RM, D'Amore PA. Transcriptional regulation of vascular endothelial growth factor in cancer. Cytokine Growth Factor Rev 2005;16: 77 – 89.

22. Finkenzeller G, Sparacio A, Technau A. Sp1 recognition sites in the proximal promoter of the human vascular endothelial growth factor gene are essential for platelet-derived growth factor-induced gene expression. Oncogene 1997;15:669 – 76.

23. Huppert JL, Balasubramanian S. G-quadruplexes in promoters throughout the human genome. Nucleic Acids Res 2007;35:406 – 13.

24. Siddiqui-Jain A, Grand CL, Bearss DJ, Hurley LH. Direct evidence for a G-quadruplex in a promoter region and its targeting with a small molecule to repress c-MYC transcription. Proc Natl Acad Sci U S A 2002;99: 11593 – 8.

25. De Armond R, Wood S, Sun D, et al. Evidence for the presence of a guanine quadruplex forming region within a polypurine tract of the hypoxia inducible factor 1α promoter. Biochemistry 2005;44:16341 – 50.

26. Sun D, Guo K, Rusche JJ, et al. Facilitation of a structural transition in the polypurine/polypyrimidine tract within the proximal promoter region of the human VEGF gene by the presence of potassium and G-quadruplex-interactive agents. Nucleic Acids Res 2005;33:6070 – 80.

27. Dexheimer TS, Sun D, Hurley LH. Deconvoluting the structural and drug-recognition complexity of the G-quadruplex-forming region upstream of the bcl-2 P1 promoter. J Am Chem Soc 2006;128:5404 – 15.

28. Cogoi S, Xodo LE. G-quadruplex formation within the promoter of the KRAS proto-oncogene and its effect on transcription. Nucleic Acids Res 2006;34:2536 – 49.

29. Shirude PS, Okumus B, Ying L, et al. Single-molecule conformational analysis of G-quadruplex formation in the promoter DNA duplex of the proto-oncogene c-kit. J Am Chem Soc 2007;129:7484 – 5.

30. Qin Y, Rezler EM, Gokhale V, et al. Characterization of the G-quadruplexes in the duplex nuclease hypersensitive element of the PDGF-A promoter and modulation of PDGF-A promoter activity by TMPyP4. Nucleic Acids Res 2007;35:7698 – 713.

31. Guo K, Pourpak A, Beetz-Rogers K, et al. Formation of pseudo-symmetrical G-quadruplex and i-motif structures in the proximal promoter region of the RET oncogene. J Am Chem Soc 2007;129:10220 – 8.

32. Dai J, Chen D, Jones RA, et al. NMR solution structure of the major G-quadruplex structure formed in the human BCL2 promoter region. Nucleic Acids Res 2006;34:5133 – 44.

33. Han H, Hurley LH, Salazar M. A DNA polymerase stop assay for G-quadruplex-interactive compounds. Nucleic Acids Res 1999;27:537 – 42.

34. Parkinson GN, Lee MP, Neidle S. Crystal structure of parallel quadruplexes from human telomeric DNA. Nature 2002;417:876 – 80.

35. Phan AT, Modi YS, Patel DJ. Propeller-type parallel-stranded G-quadruplexes in the human c-myc promoter. J Am Chem Soc 2004;126: 8710 – 16.

36. Gray DM, Gray CW, Mou TC, et al. CD of single-stranded, double-stranded, and G-quartet nucleic acids in complexes with a single-stranded DNA-binding protein. Enantiomer 2002;7:49 – 58.

37. Seenisamy J, Rezler EM, Powell TJ, et al. The dynamic character of the G-quadruplex element in the c-MYC promoter and modification by TMPyP4. J Am Chem Soc 2004;126:8702 – 9.

38. Seenisamy J, Bashyam S, Gokhale V, et al. Design and synthesis of an expanded porphyrin that has selectivity for the c-MYC G-quadruplex structure. J Am Chem Soc 2005;127:2944 – 59.

39. Kim MY, Vankayalapati H, Shin-Ya K, et al. Telomestatin, a potent telomerase inhibitor that interacts quite specifically with the human telomeric intramolecular g-quadruplex. J Am Chem Soc 2002; 124:2098 – 9.

40. Han H, Langley DR, Rangan A, et al. Selective interactions of cationic porphyrins with G-quadruplex structures. J Am Chem Soc 2001;123: 8902 – 13.

41. Ou TM, Lu YJ, Zhang C, et al. Stabilization of G-quadruplex DNA and down-regulation of oncogene c-myc by quindoline derivatives. J Med Chem 2007;50:1465 – 74.

42. Ambrus A, Chen D, Dai J, et al. Solution structure of the biologically relevant G-quadruplex element in the human c-MYC promoter. Implications for G-quadruplex stabilization. Biochemistry 2005;44:2048 – 58.

43. Yu JL, Rak JW, Klement G, Kerbel RS. Vascular endothelial growth factor isoform expression as a determinant of blood vessel patterning in human melanoma xenografts. Cancer Res 2002;62:1838 – 46.